Ab initio calculations and scanning tunneling microscopy experiments of the Si(111)-($\sqrt{7}\times\sqrt{3}$)-Pb surface

S. Brochard
Laboratoire de Métallurgie Physique, Unité Mixte de Recherche 6630 du CNRS, Université de Poitiers, SP2MI, Boîte Postale 30179, 86962 Futuroscope Chasseneuil Cedex, France

Emilio Artacho
Department of Earth Sciences, University of Cambridge, Downing Street, Cambridge CB2 3EQ, United Kingdom

O. Custance, I. Brihuega, A. M. Baró, J. M. Soler, and J. M. Gómez-Rodríguez
Departamento de Física de la Materia Condensada, Universidad Autónoma de Madrid, E-28049 Madrid, Spain
(Received 4 July 2002; published 7 November 2002)

We present first-principles electronic structure calculations combined with scanning tunneling microscopy experiments of the Si(111)-($\sqrt{7}\times\sqrt{3}$)-Pb low-temperature structure. The *ab initio* calculations have been performed with two different atomic configurations. The structure proposed from x-ray data [C. Kumpf, Surf. Sci. **448**, L213 (2000)] with 1.2 monolayer (ML) coverage is identified as the lowest energy one. The results from first-principles calculation are shown to agree well with experiment. The nature of bonding is discussed on the basis of the electronic density plots. The bonding is shown to be metallic within the lead overlayer.

DOI: 10.1103/PhysRevB.66.205403 PACS number(s): 68.35.−p, 68.43.Bc, 73.90.+f

I. INTRODUCTION

The Pb deposition on Si(111) constitutes a prototype of a metal-semiconductor interface, especially because of the low mutual bulk solubility of the two components which makes it into an excellent candidate for experimental studies. Due to the richness of the Pb/Si(111) phase diagram, a number of experimental studies by scanning tunneling microscopy (STM),[1–12] electron diffraction (LEED-RHEED),[1,5,13–18] and x-ray diffraction[19,20] have been devoted to this system in the early stages of deposition.

In particular, low coverage phases (around 1/3 monolayer) display very interesting physics, parallel to what was found for Pb on Ge(111),[21,22] and for Sn on Ge(111).[23–30] The cooling of the Pb/Si(111) system from room to low temperature results in a phase transition from the ($\sqrt{3}\times\sqrt{3}$)$R30°$ phase (that we will denote $R3$) to a (3×3) reconstruction.[11,16] At these 1/3 monolayer (ML) coverage phases, the physics seem to be related to the Pb-Si binding.

For coverage around 1 ML, another very interesting physics appears, where there is a competition between the Pb-Si interaction and the Pb-Pb interaction. This competition between two different periodicities gives rise to incommensurate phases at room temperature.[3–5,17] By cooling down the hexagonal incommensurate phase, a new phase, denoted ($\sqrt{7}\times\sqrt{3}$), has been observed by reflection high-energy electron diffraction (RHEED) (Ref. 16) and surface x-ray diffraction.[20] By means of STM, Slezák *et al.*[9] and Custance *et al.*[11] also observed the ($\sqrt{7}\times\sqrt{3}$) phase when cooling down to low temperature the (1×1) phase observed at room temperature.[1,3–5,10,12,17,31] Very recently, codepositions of Pb and Sn on a Si(111) surface have been performed in order to clarify the nature of Pb-Pb and Pb-Si bonds in this new low-temperature phase.[32,33] To gain insight into the Pb/Si(111) system a detailed understanding of this new phase is required, which is the purpose of this work.

In this paper we present detailed first-principles electronic structure calculations combined with scanning tunneling microscopy experiments of the Si(111)-($\sqrt{7}\times\sqrt{3}$)-Pb low temperature structure, whose matrix notation is $\begin{pmatrix}3 & 2\\ -1 & 1\end{pmatrix}$. This is, to our knowledge, the first electronic structure calculation reported on this phase. By ascertaining on the actual coverage of this phase, some information on the room temperature phases could be obtained. The results of this first-principles study show very satisfactory agreement with the STM experimental data presented here and with the x-ray results of Kumpf *et al.*[20] The nature of the bonding is discussed on the basis of the electronic density.

II. EXPERIMENTAL DETAILS

The experiments were carried out in an ultrahigh-vacuum (UHV) system equipped with a variable temperature scanning tunneling microscope (VT-STM), low-energy electron diffraction (LEED), Auger electron spectroscopy (AES), sample transfer and heating capabilities, a Pb evaporation cell, and a quartz crystal microbalance. The base pressure of the system is below 5×10^{-11} Torr.

Clean reconstructed Si(111)-(7×7) surfaces were obtained by flashing the samples at 1420 K, after carefully degassing at 870 K for several hours. The samples were then slowly cooled down to room temperature (RT). Si/Pb samples which presented at RT a coexistence of (1×1) and $R3$ phases were prepared by depositing ~1 ML of Pb on Si(111)-(7×7) at RT at typical rates of 0.05 ML/min [1 ML is defined as the surface atomic density of the Si(111) surface, i.e., 7.84×10^{14} atoms/cm^2], and subsequent annealing at ~720 K for 4–5 min. The samples were then transferred to the STM and slowly cooled down to temperatures as low as 40 K.

The STM experiments were carried out with a home-built variable-temperature instrument described elsewhere.[34] This

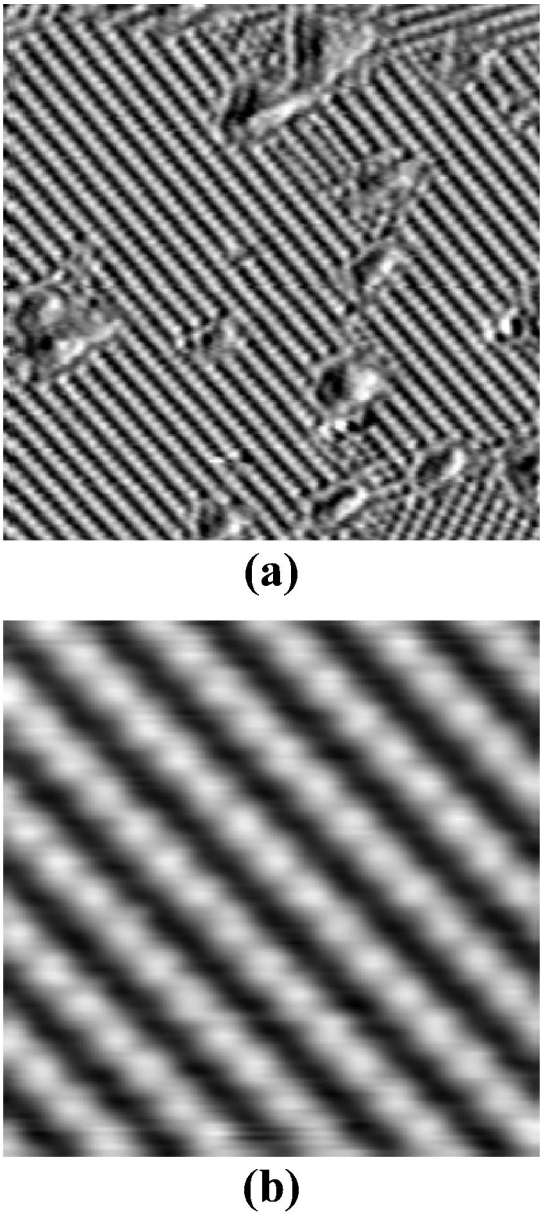

FIG. 1. Unoccupied state STM images of the $R7$ phase measured at 40 K. The image sizes are 30×30 nm^2 (a) and 7.1 $\times7.1$ nm^2 (b). The sample voltage is 1.5 V and the tunnel current is 0.2 nA for both images.

VT-STM, connected to a continuous flow liquid He UHV cryostat, allows imaging at sample temperatures in the range of 40 to 400 K. A fully automated electronics, which incorporates digital feedback control based on DSP (digital signal processor) technology, was used to operate the STM. STM data were measured in the constant current mode with variable sample voltages between -2 and $+2$ V and typical tunnel currents of 100–200 pA.

III. STM RESULTS AND ATOMIC ORGANIZATION

The Pb/Si(111)-$\begin{pmatrix} 3 & 2 \\ -1 & 1 \end{pmatrix}$ phase, which will be denoted $R7$ in the following, is obtained for Pb coverage between 0.9 and 1.2 ML from the hexagonal incommensurate (HIC) phase or

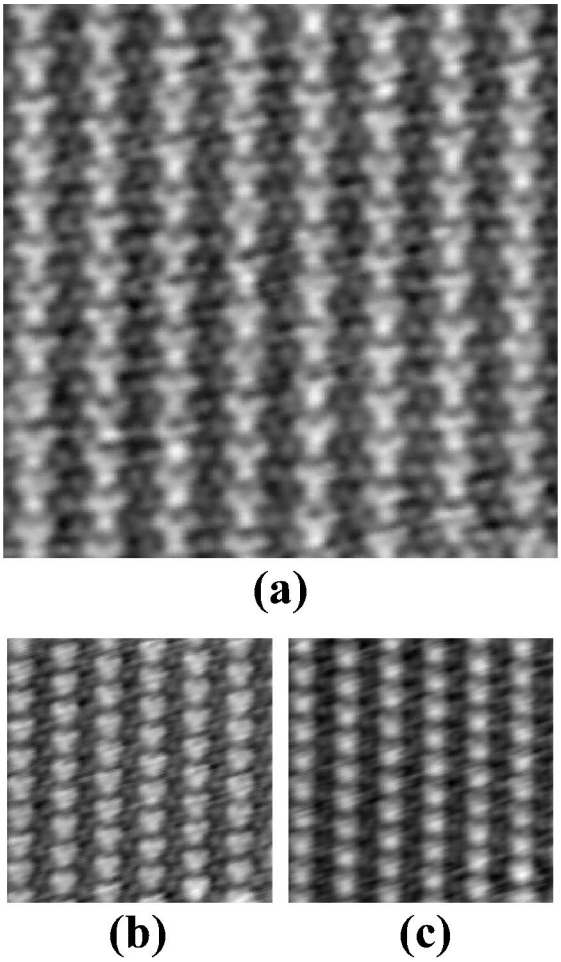

FIG. 2. High resolution occupied [(a) and (b)] and unoccupied (c) state STM images of the $R7$ phase measured at 40 K. Images (b) and (c) have been measured simultaneously. The sizes are 7.9 $\times7.9$ nm^2 (a) and 6.0×6.0 nm^2 [(b) and (c)]. The sample voltages are -1.0 V (a), -0.5 V (b), and $+1.0$ V(c). The tunnel current is 0.2 nA for all images.

from the (1×1) phase, stable at RT, when cooling down below ~250 K. Figure 1(a) displays a large scan STM image of the $R7$ phase measured at 40 K, showing the coexistence of three rotational domains. As it has been already reported,[11] typical higher magnification unoccupied-state images [Fig. 1(b)] display usually only one protrusion per unit cell. Occupied-state images, however, can present a richer intracell structure. In particular, at sample voltages in the range of around -0.5 to -1.0 V, triangular shaped protrusions can be observed in STM images as shown in Figs. 2(a) and 2(b). Simultaneously measured unoccupied-state images still reveal essentially only one diffuse protrusion per unit cell [Fig. 2(c)].

A possible interpretation of the STM images could be done on the basis of the structural model proposed by Kumpf *et al.*[20] from surface x-ray diffraction data. In this model, schematized in Fig. 3(a), the unit cell contains six Pb atoms, for a nominal lead coverage of 1.2 ML. One of the atoms (atom 1) is in a hollow site and the remaining five Pb atoms are near T_1 sites, above silicon atoms. Kumpf *et al.* de-

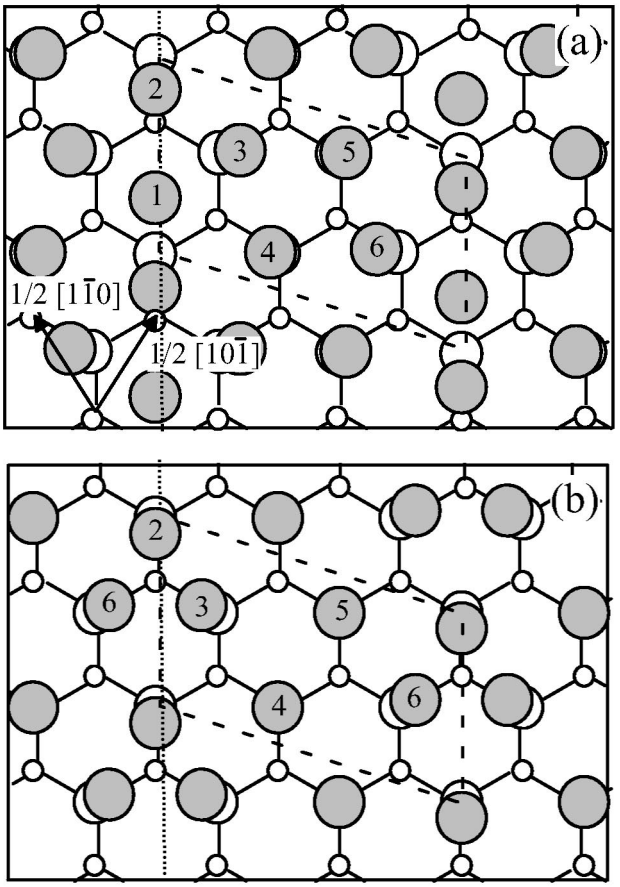

FIG. 3. Top view of the atomic models for the $R7$ phase (a) from Kumpf *et al.* (Ref. 20) and (b) trimer atomic model. Lead atoms are shown as filled gray circles; large and small open circles correspond to silicon atoms of the first double layer. The mirror plane is indicated by the dotted line, and the unit cell by the dashed line.

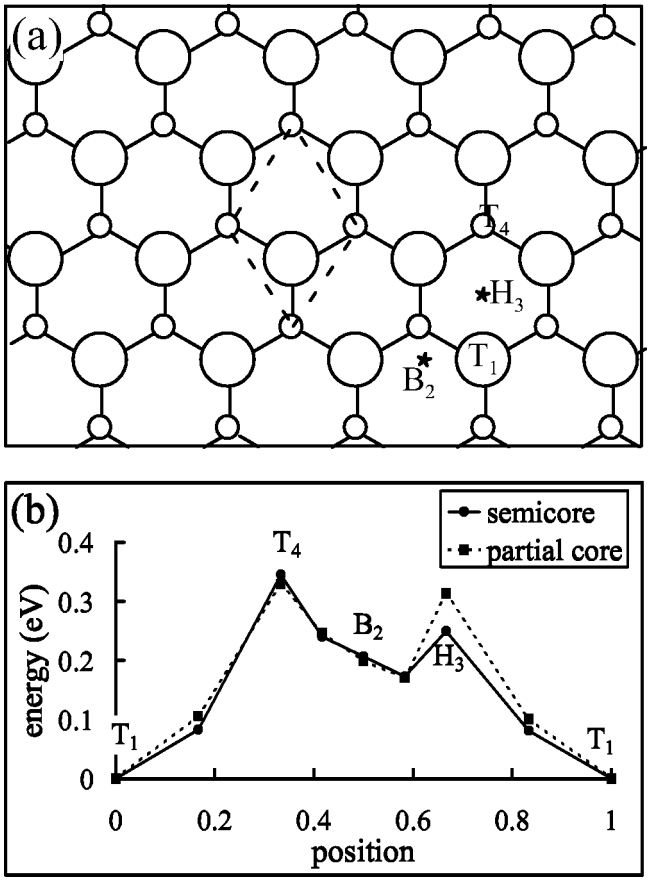

FIG. 4. (a) High-symmetry positions of the Pb adatom on the Si(111)-(1×1) structure with 1 ML Pb [the (1×1) cell is indicated by the dashed line] and (b) corresponding energies relative to the lowest-energy site (T_1), calculated with partial core corrected pseudopotential or by including semicore electrons into the valence for lead.

scribed Pb atom 2 as on a bridge position but we do not consider this justified since only one of the two silicon atoms below (the closest one) has a dangling bond. The coordination of atom 1 is markedly different from that of the other lead atoms,[11,20] so that the local density of states around it should also be significantly different. Consequently, the triangular structure observed in Fig. 2 could correspond to the group of atoms 1, 2, 3, and 6, centered on atom 1.

Nevertheless, other alternative interpretation of the triangular features observed in occupied-state STM images could be proposed. In particular, a naive view of the STM data could associate each protrusion in these images with just one Pb atom. In this way, the bright triangular features observed in occupied-state images would correspond to a Pb trimer, while the other two remaining protrusions [see Fig. 2(a)] would correspond to two Pb atoms. The formation of Pb trimers has already been proposed by Hwang *et al.* as a possible interpretation of the STM images measured at room temperature on the Pb/Si(111) incommensurate phases[3] and on the Pb/Ge(111) $\beta-(\sqrt{3}\times\sqrt{3})R30°$ phase.[35,36] Moreover, it has been suggested, very recently, that these kind of trimers could be the building blocks of most of the dense Pb/Si(111) reconstructions.[18]

To investigate whether the structural model proposed by Kumpf *et al.*[20] is indeed the most stable configuration for the $R7$ structure, we have performed first-principles calculations of this model and of another atomic organization, which can be described as a trimer model. In the trimer model, only five lead atoms belong to the unit cell, for a lead coverage of 1 ML. Lead atoms are basically in T_1 on-top sites [Fig. 3(b)], and the trimer is formed by atoms 2, 3, and 6, which displaced from the perfect T_1 positions would form the bright triangular structure observed in Fig. 2. We consider these arrangements as the most likely ones for this system, the first one motivated by the x-ray data, the second one motivated by known patterns of trimers in the Pb/Ge(111) and Pb/Si(111) systems.

For both models (x-ray and trimer), the surface energy have been determined and compared to the surface energy of the $R3$ phase. The phase appearing at lower coverage than the ones studied here is known to have a coverage of 1/3 ML and a (3×3) reconstruction. In this work we use the $R3$ phase as reference instead of the (3×3) since only its surface energy is needed for our purposes, which does not

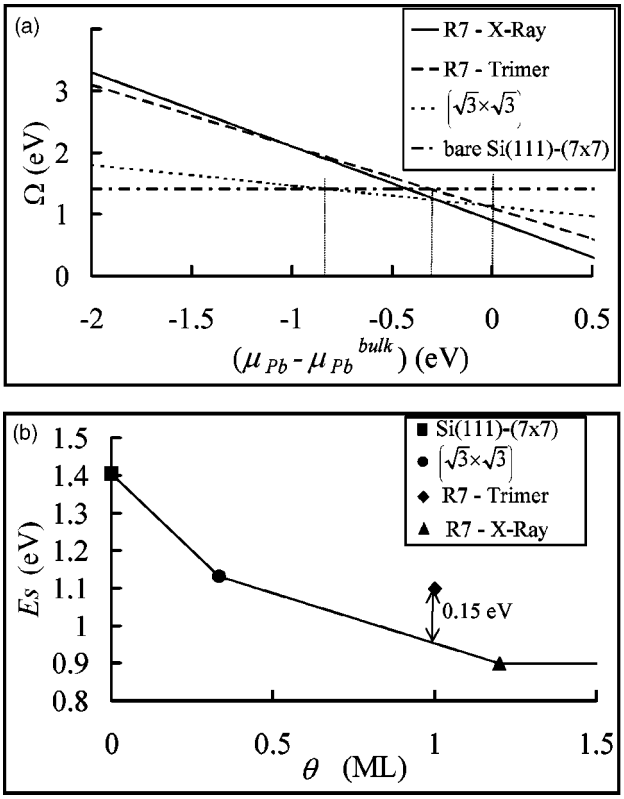

FIG. 5. (a) Surface formation free energy per unit (1×1) surface cell as a function of lead chemical potential as defined by Eq. (1) and (b) reduced surface energy versus coverage as defined by Eq. (2) for the different phases (the horizontal line corresponds to the appearance of bulklike clusters). The energy of the bare Si(111)-(7×7) surface has been calculated with the Siesta method under the approximations described in Sec. IV.

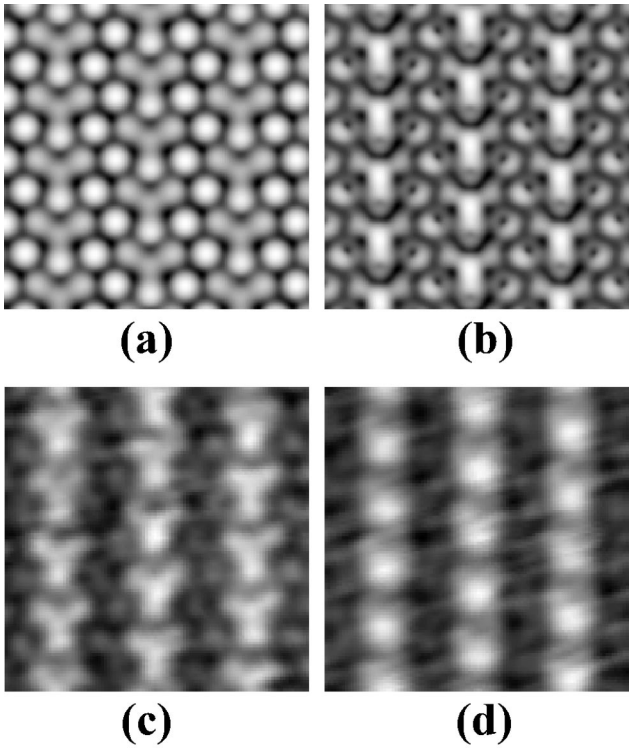

FIG. 6. Local density of states obtained from the SIESTA calculation integrated between (a) the Fermi level (E_F) and $E_F - 1.0$ eV (b) E_F and $E_F + 1.0$ eV. STM images obtained for a tunnel current of 0.2 nA and sample voltages (c) -1.0 V and (d) $+1$ V. The image size is 3.2×3.2 nm^2. The calculated images correspond to isosurfaces of constant LDOS (5×10^{-4} atomic units) and their intensity has been linearly coded according to the vertical height from black (low) to white (high).

change substantially between the two 1/3 ML phases, as calculated for the Pb/Ge(111) and Sn/Ge(111) systems. [The energy difference between the two phases is lower than 0.02 eV/(1×1) unit cell.][21,28,37]

IV. COMPUTATIONAL METHOD

The *ab initio* calculations performed are based on the density-functional theory[38] in its local density approximation for exchange and correlation potentials.[39,40] The Siesta method[41,42] used to calculate the energy and atomic forces uses separable[43] norm-conserving Troullier-Martins[44] pseudopotentials. The valence wave functions are expanded on pseudoatomic orbitals including multiple-ζ and polarization functions.[42]

The repeated unit cell was made of one layer of lead atoms, twelve layers of silicon and a layer of hydrogen atoms saturating the dangling bonds of the last (bulklike) silicon layer. Both the last silicon layer and the hydrogen layer were kept fixed during relaxation, the H-Si distance being determined by a previous calculation in a bulklike slab saturated in both sides. The remaining eleven Si layers, and lead atoms were allowed to relax freely. Slabs were separated by more than 20 Å.

A uniform real-space grid with an equivalent plane-wave cutoff of 100 Ry was used for numerical integration.[45] For improving grid-cutoff convergence, we made a grid cell sampling (with rigid displacements of the system with respect to the grid), which enables a symmetrization of energy and force terms that depend on the grid. Integrations over the first Brillouin zone were replaced by finite sums with a *k*-grid cutoff[46] of 15 Å, which implied 9 *k* points. The total system energy at zero temperature was relaxed using a conjugate gradient method. The relaxation was assumed to be finished when the maximum residual force was below 0.04 eV/Å.

For the lead pseudopotential, we used a partial core correction to treat the nonlinear exchange and correlation interaction between the core and valence charge densities.[47] This insures a better transferability of the pseudopotential in comparison with a pure valence pseudopotential, and a limited computational time in comparison with a semicore pseudopotential containing 5*d* electrons. To obtain satisfactory results, we used a partial core radius r_{pc} of 1.5 Bohr. Below this value, and with a pure valence pseudopotential, a discontinuity on the total energy versus bulk parameter curve appeared for lead in its bulk form, discontinuity that could only be removed with a high mesh cutoff. The reliability of the lead pseudopotential has been tested on a Pb/Si(111)-(1×1) surface with 1 ML of Pb. In Fig. 4(a), the high-

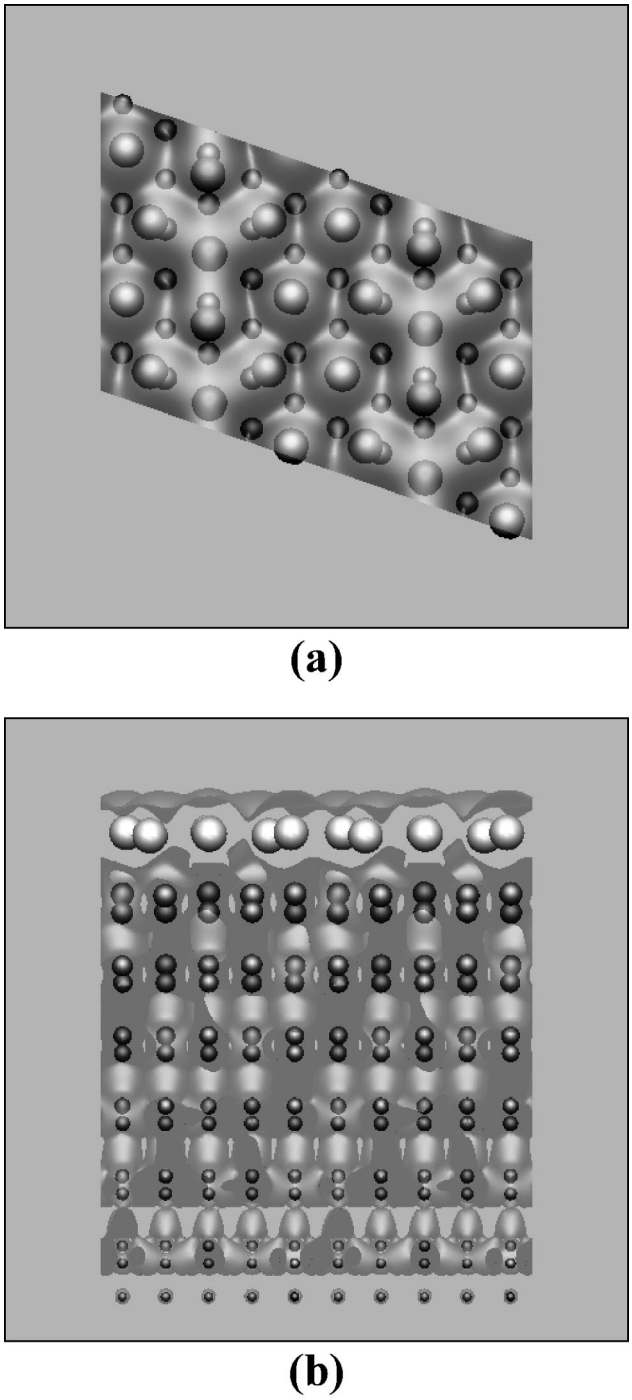

FIG. 7. Top view (a) and side view (b) of the LDOS calculated with SIESTA integrated between E_F and $E_F-0.5$ eV. Shaded views of isosurfaces of constant LDOS (5×10^{-4} atomic units) are displayed together with the relaxed atomic positions of the atoms represented by spheres of different sizes (Pb: large spheres; Si: spheres with decreasing size as the depth of the layer increases; H: smallest spheres). These data as well as those in Fig. 6 and all the STM data have been displayed with the WSXM software (Ref. 53).

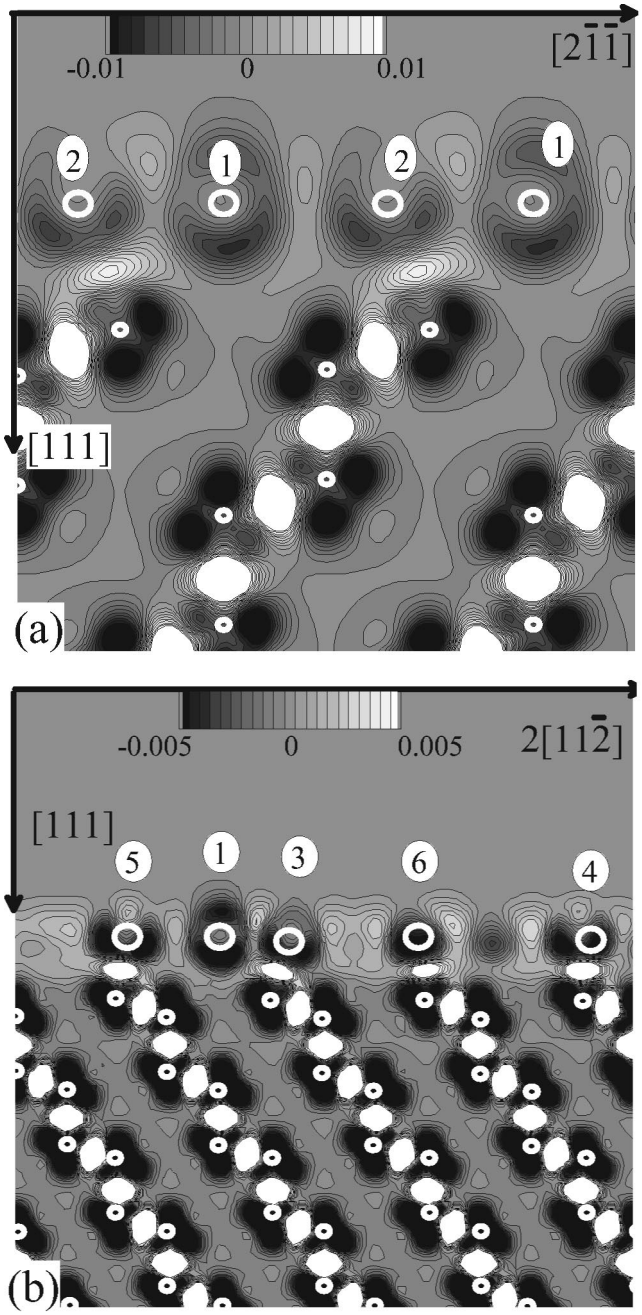

FIG. 8. Deformation density [Eq. (3)] in (a) plane $(01\bar{1})$ and (b) plane $(1\bar{1}0)$. Both planes are normal to the surface plane (see cut directions in Fig. 9). Large (small) white open circles denote Pb (Si) atoms contained in the cut planes. Pb atom numbers are indicated. The unit is in electron charges per Bohr^3. A covalent bond is evidenced by a maximum of the electronic density between two atoms.

symmetry positions for the Pb adatoms on the Si(111)-(1 $\times$1) surface are indicated. The corresponding energies relative to the lowest-energy site (T_1), as well as intermediate ones, have been calculated both with the partial core (r_{pc} $=1.5$ Bohrs) corrected lead pseudopotential and by including semicore electrons explicitely in the valence. They are shown in Fig. 4(b), where it can be seen that energies with partial and semicore pseudopotentials compare very well, the largest discrepancy (for the H_3 site) being smaller than 0.07 eV.

For silicon and lead, we used a double-ζ polarized basis set of numerical atomic orbitals optimized variationally with

TABLE I. Atomic positions from Siesta in the $R7$-x-ray structure and comparison with experimental data. (Ref. 20). Atomic positions refer to the basis $\mathbf{a}=\frac{1}{2}[10\bar{1}]$, $\mathbf{b}=\frac{1}{2}[\bar{1}10]$, $\mathbf{c}=\frac{1}{2}[111]$ [see Fig. 3(a)]. The atomic positions marked 1 and 1a correspond to two possible fits of the experimental data reported by Kumpf *et al.*

Atom	Position from Ref. 20	Position from Siesta	Difference
Pb 1	-0.294, 0.294, 0.832	}-0.344, 0.323, 0.875	0.050, 0.029, -0.043
Pb 1a	-0.294, 0.294, 1.024		0.050, 0.029, 0.149
Pb 2	-0.839, 0.839, 0.890	-0.875, 0.871, 0.902	-0.018, 0.038, -0.012
Pb 3	0.163, 1.228, 0.942	0.135, 1.228, 0.853	-0.028, 0.000, 0.089
Pb 4	0.923, 0.960, 0.880	0.924, 0.979, 0.900	0.001, 0.019, -0.020
Pb 5	1.040, 2.077, 0.880	0.994, 2.094, 0.898	-0.046, 0.017, -0.018
Pb 6	1.772, 1.837, 0.942	1.743, 1.858, 0.853	-0.029, 0.021, 0.089
Si	-0.007, 0.007, 0.050	0.000, -0.001, 0.039	0.007, -0.008, 0.011
Si	0.006, 1.044, 0.015	0.003, 1.006, 0.004	-0.003, -0.038, 0.011
Si	0.998, 1.028, 0.035	0.999, 1.002, 0.028	0.001, -0.026, 0.007
Si	0.972, 2.002, 0.035	0.994, 1.999, 0.030	0.022, -0.003, 0.005
Si	1.956, 1.994, 0.015	1.993, 1.996, 0.007	0.037, 0.002, 0.008
Si	-0.675, 0.675, -0.273	-0.670, 0.668, -0.234	0.005, -0.007, -0.039
Si	0.338, 0.693, -0.227	0.335, 0.665, -0.228	-0.003, -0.028, 0.001
Si	0.328, 1.704, -0.244	0.334, 1.674, -0.245	0.006, -0.030, 0.001
Si	1.296, 1.672, -0.244	1.324, 1.663, -0.241	0.028, -0.007, -0.003
Si	2.307, 1.662, -0.227	2.333, 1.663, -0.226	0.026, 0.001, -0.001

a flexible confinement scheme.[48] For hydrogen saturators we used a simpler single-ζ basis set.

V. SIMULATION RESULTS

The surface formation free energy [per (1×1) surface unit] at zero temperature is defined as[49,50]

$$\Omega=\frac{1}{n}(E_{\mathrm{slab}}-n_{\mathrm{H}}E_{\mathrm{H}}^{\mathrm{sat}}-n_{\mathrm{Si}}\mu_{\mathrm{Si}}^{\mathrm{bulk}}-n_{\mathrm{Pb}}\mu_{\mathrm{Pb}}),$$

where n is the number of Si atoms per layer in a slab unit cell ($n=3$ for the $R3$ structure; $n=5$ for the $R7$ structure), E_{slab} is the energy of the slab system per slab unit cell, n_{H}, n_{Si}, and n_{Pb} are, respectively, the number of hydrogen atoms saturating the back surface, the number of silicon substrate atoms, and the number of lead atoms per slab unit cell, $E_{\mathrm{H}}^{\mathrm{sat}}$ is the energy per saturating hydrogen atom (obtained from a previous calculation in a bulklike saturated slab), $\mu_{\mathrm{Si}}^{\mathrm{bulk}}$ is the energy per Si atom in its bulk form, and μ_{Pb} is the chemical potential of lead. The surface formation free energy can be rewritten

$$\Omega=\frac{E_{\mathrm{slab}}}{n}-E_{\mathrm{H}}^{\mathrm{sat}}-n_{\mathrm{layer}}\mu_{\mathrm{Si}}^{\mathrm{bulk}}-\theta\mu_{\mathrm{Pb}}^{\mathrm{bulk}}-\theta(\mu_{\mathrm{Pb}}-\mu_{\mathrm{Pb}}^{\mathrm{bulk}}), \tag{1}$$

n_{layer} being the number of silicon layers in the slab used (here $n_{\mathrm{layer}}=12$), θ the lead coverage, and $\mu_{\mathrm{Pb}}^{\mathrm{bulk}}$ the chemical potential of lead in its bulk form. E_{slab}, $\mu_{\mathrm{Si}}^{\mathrm{bulk}}$, $E_{\mathrm{H}}^{\mathrm{sat}}$, and $\mu_{\mathrm{Pb}}^{\mathrm{bulk}}$ have been determined under the approximations described in Sec. IV.

In Fig. 5(a), the curves representing Ω as a function of $\mu_{\mathrm{Pb}}-\mu_{\mathrm{Pb}}^{\mathrm{bulk}}$ are straight lines with slope $\theta=1/3$ for the $R3$ structure, $\theta=1.2$ for the $R7$-x-ray structure and $\theta=1$ for the $R7$-trimer structure. From Fig. 5(a), it is seen that the $R3$ reconstruction is the most stable structure for $\mu_{\mathrm{Pb}}-\mu_{\mathrm{Pb}}^{\mathrm{bulk}}$ lower than -0.27 eV, then the $R7$-x-ray structure is the most stable one until μ_{Pb} becomes equal to $\mu_{\mathrm{Pb}}^{\mathrm{bulk}}$ (when Pb clusters are expected to start growing on the surface). The $R7$-trimer structure is thus never stable. The energies of the different phases can also be compared using the coverage θ as fundamental variable instead of μ_{Pb}, which allows a more direct comparison to experiment. In Fig. 5(b), we have plotted a reduced surface energy defined as

$$E_S=\frac{E_{\mathrm{slab}}}{n}-E_{\mathrm{H}}^{\mathrm{sat}}-n_{\mathrm{layer}}\mu_{\mathrm{Si}}^{\mathrm{bulk}}-\theta\mu_{\mathrm{Pb}}^{\mathrm{bulk}}, \tag{2}$$

where the term $-\theta\mu_{\mathrm{Pb}}^{\mathrm{bulk}}$ has been added for clarity. In this plot, the curve joining the points representing stable saturated surface structures must be convex.[51] The point representing the $R7$-trimer phase lying above the curve, this phase is therefore unstable. Furthermore, in Fig. 5(b), the arrow indicates the range of instability of the $R7$-trimer phase; the value of 0.15 eV is larger than the typical error of the *ab initio* calculation, confirming the stability of the $R7$-x-ray versus the $R7$-trimer structure. As a matter of fact, an analysis of the atomic positions after relaxation when starting from the trimer model shows that this structure goes back to an almost perfect (1×1) surface.

The relaxed atomic positions obtained from the simulation when starting from the x-ray model are presented in Table I, together with the experimental data.[20] As can be seen

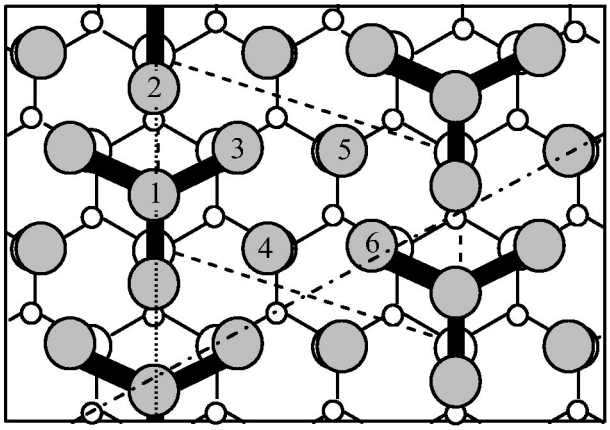

FIG. 9. Top view of the $R7$-x-ray phase. Distances between lead atoms lower than 3.15 Å are shown as black bars. The other distances between lead atoms are greater than 3.25 Å. The dotted line (mirror line) indicates the intersection between the surface and the cut plane shown in Fig. 8(a). The dot-dashed line indicates the intersection between the surface and the cut plane shown in Fig. 8(b).

from Table I, the positions obtained from Siesta compare well with the experimental ones. It should be noted that the silicon bulk lattice parameter in the simulation is 5.38 Å, while the experimental one is 5.43 Å.

The local density of states (LDOS) resulting from the calculations has been computed: this allows the plot of simulated STM images[52] which can be compared to the experimental STM images. Figure 6 displays both, calculated and experimental occupied and unoccupied state images. Although some differences in the relative intensities can be noted, Fig. 6 emphasizes the good agreement between experiments and *ab initio* calculations. In particular, the triangular structure (Y-like form) appears clearly in both simulated and experimental occupied state images. This structure is much more diffuse in unoccupied state images, resulting in experimental STM images in just one diffuse protrusion per unit cell. In order to ensure that the Y-shaped features correspond to the group of atoms 1, 2, 3, 6 (where 1 is in the center of the Y), the relaxed positions of the atoms have been plotted together with top and side views of the LDOS and are displayed in Fig. 7. This figure illustrates that there is a perfect match between Y protrusions and the abovementioned group of atoms.

VI. DISCUSSION

In previous papers,[20,33] assumptions on the nature of bonding between lead and silicon atoms have been proposed. Kumpf *et al.* interpreted bonding in terms of the interatomic distances. The first feature noticed by Kumpf *et al.* concerns the distances between each lead atom and its next silicon atom. Their experimental data (as well as our *ab initio* results) show that these distances are significantly smaller for Pb atoms 2, 3, 4, 5, and 6 than for Pb atom 1. The distances of Pb atoms 2, 3, 4, 5, and 6 to the next silicon atom are either close to the sum of Pb and Si covalent radii (2.65 Å) or close to the sum of the covalent radius of Si with the

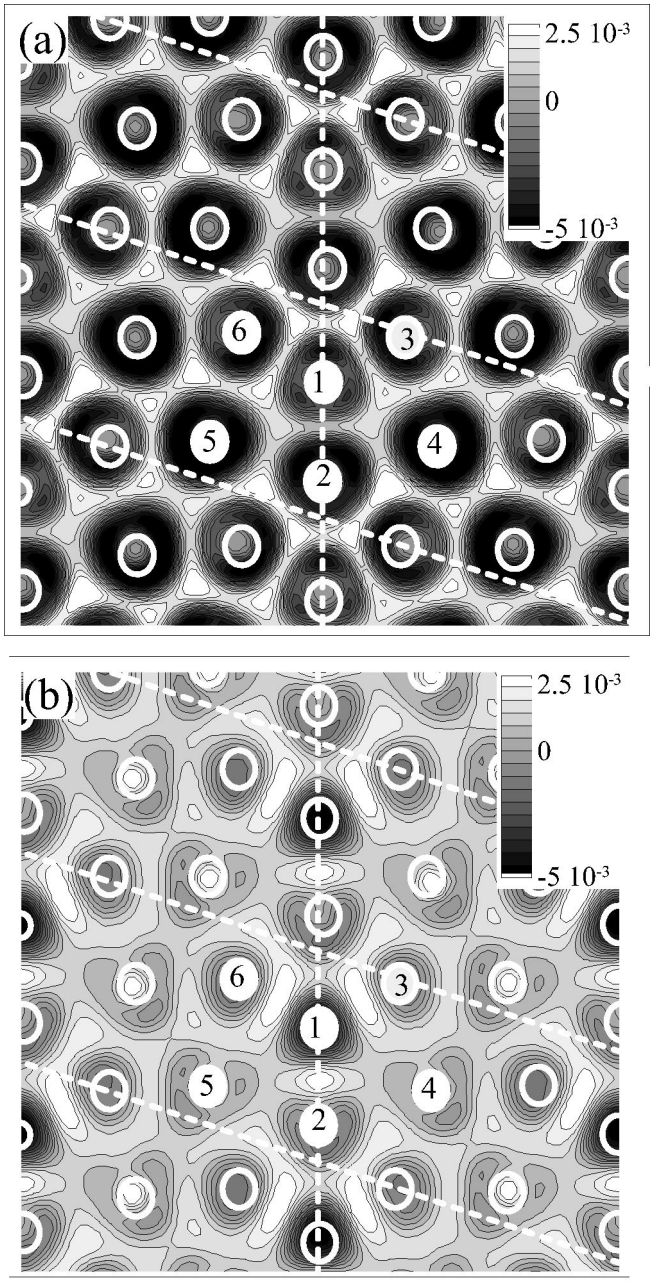

FIG. 10. Deformation density as defined by Eq. (3) (a) in the lead atoms plane (defined as the plane parallel to the surface midway between Pb atoms 3 and 6 and Pb atom 2) and (b) one Å above. White circles denote Pb atoms. Pb atom numbers are indicated. The white dashed line indicates the $R7$ unit cell. The unit is in electron charges per Bohr^3.

radius in bulk Pb (2.93 Å). It has thus been proposed by Kumpf *et al.*[20] that lead atoms 2, 3, 4, 5, and 6 form a covalent bond with substrate silicon atoms, saturating all the dangling bonds of the silicon substrate, while Pb atom 1 forms no covalent bond with silicon, which could explain the scattered experimental data for the position of this atom along the [111] direction. To check this assumption, we have performed plots of the electronic density obtained from the *ab initio* calculation. In Fig. 8, contour plots of the deformation density

$$\Delta\rho(\mathbf{r}) = \rho_{R7}(\mathbf{r}) - \sum_{i}^{\text{atoms}} \rho_i^{\text{at}}(\mathbf{r}) \quad (3)$$

are presented, where $\rho_{R7}(\mathbf{r})$ is the valence electronic density at point $\mathbf{r}$ in the Pb/Si(111)-$R7$-x-ray relaxed configuration, and $\rho_i^{\text{at}}(\mathbf{r})$ is the valence atomic electronic density of an isolated atom (Pb or Si). Figure 8 displays $\Delta\rho(\mathbf{r})$ in two cut planes normal to the (111) surface, containing both lead and silicon atoms. Figure 8(a) shows that the Pb atom labeled as 2 indeed forms a covalent bond with the silicon substrate, while Pb atom 1 does not. In Fig. 8(b), the covalent bonding between lead atoms 3, 4, 5, 6 and the silicon atoms is also evident, everything so far in agreement with the analysis of Kumpf *et al.*

The second point discussed by Kumpf *et al.*[20] is the nature of Pb-Pb bonds in the lead overlayer. Figure 9 summarizes Kumpf's analysis: distances similar to the covalent Pb-Pb bond length of 2.94 Å only occur around atom 1, whereas distances close to the bond length in metallic lead (3.50 Å) occur around all other atoms. This led Kumpf *et al.* to suggest that Pb atom 1 forms a covalent bond with its three closest neighbors (2, 3, and 6) while the others Pb-Pb bonds are of metallic character. This interpretation would also correctly explain the bright structure seen on STM images (Figs. 2 and 6). In Fig. 10, the charge density $\Delta\rho(\mathbf{r})$ as obtained from the ab initio calculation has been represented in the lead atoms plane (defined as the plane parallel to the surface midway between Pb atoms 3 and 6 and Pb atom 2). In Fig. 10(a), a covalent bond between Pb atoms would be evidenced by a maximum of the electronic density between two atoms, which is clearly not the case. $\Delta\rho(\mathbf{r})$ is never maximum between two atoms, but in the interstitial zones between three atoms, such as, for example, between atoms 1, 5, and 6. In addition, in Fig. 10(b), it is seen that a maximum of the charge density occurs between atom 1 and its three closest Pb neighbors above the lead atoms plane. This is confirmed in Fig. 8, where the maximum of $\Delta\rho(\mathbf{r})$ between Pb atoms is not in the atoms plane but above or below it. The charge distribution obtained from our *ab initio* calculation is then consistent with a metallic bonding between all the Pb atoms, showing that a description based on covalent bonds within the lead overlayer would be inappropriate. The smaller Pb-Pb distances of atom 1 should be attributed to the lack of bonds between this atom and the silicon substrate. This effect is typical of metals, where the reduced coordination explains the reduction of surface interatomic distances and many surface reconstructions. The lack of Pb-Si bonds produces also a larger redistribution of charge in the Pb-Pb bonds of atom 1 and it explains the bright structure seen on the STM images.

VII. CONCLUSION

We have performed first-principles electronic structure calculations and STM experiments for the low-temperature Si(111)-($\sqrt{7}\times\sqrt{3}$)-Pb phase, finding a very satisfactory agreement. The atomic structure of this phase has been identified to the one proposed from surface x-ray diffraction data[20] rather than a trimer model resulting from a naive interpretation of STM images. We have thus determined the actual coverage of this phase (1.2 ML). The simulated STM images compare also very well with the experimental ones.

The electronic density plots, obtained from the *ab initio* calculation, provide information on the bonds between the surface atoms constituting this phase. We have confirmed the existence of covalent bonds between five of the Pb atoms belonging to the ($\sqrt{7}\times\sqrt{3}$) unit cell and substrate silicon atoms, yielding a saturation of all the dangling bonds of the silicon substrate. The bonding inside the lead overlayer has been found somewhat different from previous analyses based on interatomic distances.[20,33] We have shown that all bonds between lead atoms are of metallic character.

ACKNOWLEDGMENTS

We thank Javier Junquera and Eduardo Anglada for providing us with optimized basis for silicon and lead. Fruitful discussions with J. Gómez Herrero are gratefully acknowledged. This work was supported in part by CAM (Contract No. 07N/0054/2001). This work was performed with the support of the Spanish Ministerio de Ciencia y Tecnología under Grant No. BFM2000-1312. S. B. acknowledges partial financial support from NATO during her stay at the Universidad Autónoma de Madrid.

[1] E. Ganz, F. Xiong, I. S. Hwang, and J. Golovchenko, Phys. Rev. B **43**, 7316 (1991).
[2] D. Tang, H. E. Elsayed-Ali, J. Wendelken, and J. Xu, Phys. Rev. B **52**, 1481 (1995).
[3] I. S. Hwang, R. E. Martinez, C. Liu, and J. A. Golovchenko, Phys. Rev. B **51**, 10 193 (1995).
[4] I. S. Hwang, R. E. Martinez, C. Liu, and J. A. Golovchenko, Surf. Sci. **323**, 241 (1995).
[5] L. Seehofer, G. Falkenberg, D. Daboul, and R. L. Johnson, Phys. Rev. B **51**, 13 503 (1995).
[6] J. M. Gómez-Rodríguez, J. J. Sáenz, A. M. Baró, J. Y. Veuillen, and R. C. Cinti, Phys. Rev. Lett. **76**, 799 (1996).
[7] J. M. Gómez-Rodríguez, J. Y. Veuillen, and R. C. Cinti, Surf. Sci. **377-379**, 45 (1997).
[8] J. Y. Veuillen, J. M. Gómez-Rodríguez, A. M. Baró, and R. C. Cinti, Surf. Sci. **377-379**, 847 (1997).
[9] J. Slezák, P. Mutombo, and V. Cháb, Phys. Rev. B **60**, 13 328 (1999).
[10] J. Slezák, P. Mutombo, and V. Cháb, Surf. Sci. **454-456**, 584 (2000).
[11] O. Custance, J. M. Gómez-Rodríguez, A. M. Baró, L. Juré, P. Mallet, and J. Y. Veuillen, Surf. Sci. **482-485**, 1399 (2001).
[12] O. Custance, I. Brihuega, J. Y. Veuillen, J. M. Gómez-Rodríguez, and A. M. Baró, Surf. Sci. **482-485**, 878 (2001).

[13] H. H. Weitering, D. R. Heslinga, and T. Hibma, Phys. Rev. B **45**, 5991 (1992).
[14] P. J. Estrup and J. Morisson, Surf. Sci. **2**, 465 (1964).
[15] H. Yaguchi, S. Baba, and A. Kinbara, Appl. Surf. Sci. **33-34**, 1025 (1988).
[16] K. Horikoshi, X. Tong, T. Nagao, and S. Hasegawa, Phys. Rev. B **60**, 13 287 (1999).
[17] X. Tong, K. Horikoshi, and S. Hasegawa, Phys. Rev. B **60**, 5653 (1999).
[18] A. Petkova, J. Wollschäleger, H. L. Günter, and M. Henzler, Surf. Sci. **471**, 11 (2001).
[19] K. A. Edwards, P. B. Howes, J. E. Macdonald, T. Hibma, T. Bootsma, and M. A. James, Surf. Sci. **424**, 169 (1999).
[20] C. Kumpf, O. Bunk, J. H. Zeysing, M. M. Nielsen, M. Nielsen, R. L. Johnson, and R. Feidenhans'l, Surf. Sci. **448**, L213 (2000).
[21] J. M. Carpinelli, H. H. Weitering, E. W. Plummer, and R. Stumpf, Nature (London) **381**, 398 (1996).
[22] A. Goldoni, C. Cepek, and S. Modesti, Phys. Rev. B **55**, 4109 (1997).
[23] O. Bunk, J. H. Zeysing, G. Falkenberg, R. L. Johnson, M. Nielsen, M. M. Nielsen, and R. Feidenhans'l, Phys. Rev. Lett. **83**, 2226 (1999).
[24] J. M. Carpinelli, H. H. Weitering, M. Bartkowiak, R. Stumpf, and E. W. Plummer, Phys. Rev. Lett. **79**, 2859 (1997).
[25] A. Goldoni and S. Modesti, Phys. Rev. Lett. **79**, 3266 (1997).
[26] A. P. Baddorf, V. Jahns, J. Zhang, J. M. Carpinelli, and E. W. Plummer, Phys. Rev. B **57**, 4579 (1998).
[27] R. I. G. Uhrberg and T. Balasubramanian, Phys. Rev. Lett. **81**, 2108 (1998).
[28] J. Avila, A. Mascaraque, E. G. Michel, M. C. Asensio, G. LeLay, J. Ortega, R. Pérez, and F. Flores, Phys. Rev. Lett. **82**, 442 (1999).
[29] J. Zhang, Ismail, P. J. Rous, A. P. Baddorf, and E. W. Plummer, Phys. Rev. B **60**, 2860 (1999).
[30] H. H. Weitering, J. M. Carpinelli, A. V. Melechko, J. Zhang, M. Bartkowiak, and E. W. Plummer, Science **285**, 2107 (1999).
[31] A. J. Caamaño, Y. Pogorelov, O. Custance, J. Méndez, A. M. Baró, J. Y. Veuillen, J. M. Gómez-Rodríguez, and J. J. Sáenz, Surf. Sci. **426**, L420 (1999).
[32] J. Yuhara, D. Nakamura, K. Soda, and K. Morita, Surf. Sci. **482-485**, 1374 (2001).
[33] C. Kumpf, M. Nielsen, R. Feidenhans'l, Y. Su, and R. L. Johnson, Surf. Sci. **486**, L495 (2001).
[34] O. Custance, Ph.D. thesis, Universidad Autónoma de Madrid, 2002.
[35] I. S. Hwang and J. A. Golovchenko, Phys. Rev. Lett. **71**, 255 (1993).
[36] I. S. Hwang and J. A. Golovchenko, Phys. Rev. B **50**, 18 535 (1994).
[37] S. de Gironcoli, S. Scandolo, G. Ballabio, G. Santoro, and E. Tosatti, Surf. Sci. **454-456**, 172 (2000).
[38] W. Kohn and L. Sham, Phys. Rev. **140**, 1133 (1965).
[39] D. M. Ceperley and B. J. Alder, Phys. Rev. Lett. **45**, 566 (1980).
[40] J. P. Perdew and A. Zunger, Phys. Rev. B **23**, 5048 (1981).
[41] D. Sánchez-Portal, P. Ordejón, E. Artacho, and J. M. Soler, Int. J. Quantum Chem. **65**, 453 (1997).
[42] J. M. Soler, E. Artacho, J. D. Gale, A. García, J. Junquera, P. Ordejón, and D. Sánchez-Portal, J. Phys.: Condens. Matter **14**, 2745 (2002).
[43] L. Kleinman and D. M. Bylander, Phys. Rev. Lett. **48**, 1425 (1982).
[44] N. Troullier and J. L. Martins, Phys. Rev. B **43**, 1993 (1991).
[45] P. Ordejón, E. Artacho, and J. M. Soler, Phys. Rev. B **53**, R10 441 (1996).
[46] J. Moreno and J. M. Soler, Phys. Rev. B **45**, 13 891 (1992).
[47] S. G. Louie, S. Froyen, and M. L. Cohen, Phys. Rev. B **26**, 1738 (1982).
[48] J. Junquera, O. Paz, D. Sánchez-Portal, and E. Artacho, Phys. Rev. B **64**, 235111 (2001).
[49] R. D. Meade and D. Vanderbilt, Phys. Rev. Lett. **63**, 1404 (1989).
[50] J. E. Northrup, Phys. Rev. B **44**, 1419 (1991).
[51] E. Artacho and J. Zegenhagen, Phys. Rev. B **52**, 16 373 (1995).
[52] J. Tersoff and D. R. Hamann, Phys. Rev. Lett. **50**, 1998 (1983).
[53] WSxM free software downloadable at http://www.nanotec.es.